2023 IEEE International Conference on Robotics and Automation (ICRA 2023)
May 29 - June 2, 2023. London, UK

Dimensional Optimization and Anti-Disturbance Analysis of an Upgraded Feed Mechanism in FAST

Xiaoyan Wang[1], Bin Zhang[1*], Zhaoyang Li[1], Xinyu Gao[1], Fei Zhang[1], Yifan Ma[1], Rui Yao[2], Jia-Ning Yin[2], Hui Li[2], Qingge Yang[2], Qingwei Li[2], and Weiwei Shang[1]

***Abstract*— Five-hundred-meter aperture spherical radio telescope (FAST) is a very famous large-scale scientific facility with excellent performance for astronomical observation in the world, but it currently fails to observe the center of the Milky Way Galaxy due to the limited observation angle that is affected by the heavy weight of the feed cabin. To improve this problem, an upgraded feed mechanism (UFM) with a lighter cable structure is designed and employed to replace the existing heavy rigid A-B rotator and Stewart platform in the feed cabin of FAST. The structural dimension of the UFM is analyzed and optimized under cable tension constraints to meet the requirements of the observation angle. Then, a novel disturbance increment method is proposed to analyze the anti-disturbance ability of the UFM, where a gradually increased disturbance wrench is applied to the UFM with the stiffness matrix iteratively updated. Through the dimensional optimization and further anti-disturbance analysis, the newly-designed UFM can indeed meet the higher demand for astronomical observation with the larger observation angle, which benefits from the lightweight cable structure. Besides, the UFM also has the appreciable anti-disturbance ability for long-term stable operation of FAST.**

I. Introduction

Five-hundred-meter aperture spherical radio telescope (FAST) is the largest and most sensitive single-aperture radio telescope in the world. Based on the abilities of large receiving area, accurate tracking, and multi-beam reception, it has become a powerful tool in the field of medium-low frequency radio astronomy, such as pulsar search, neutral hydrogen observation, and dark matter detection, etc. [1]–[4].

FAST is mainly composed of a main reflector, a six-cable-driven mechanism (SCDM), and a feed cabin with multiple feed receivers (see Figs. 1(a)(b)), where the SCDM is used to control the feed cabin to track the electromagnetic waves converged by the main reflector. The feed cabin consists of a star frame, an A-B rotator, and a Stewart platform [5]. The former one is a metal frame that is used to support the heavy components, and the latter two are controlled to further compensate for the remaining angle and tracking errors, respectively. Then, under the two-level control, the feed receivers installed on the Stewart platform can have satisfactory tracking accuracy in receiving the waves [6].

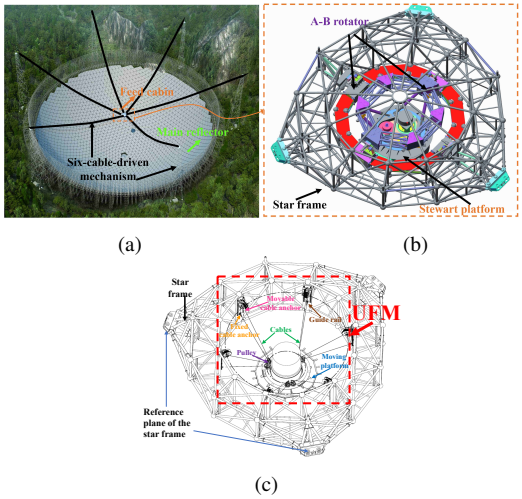

Fig. 1. (a) Six-cable-driven mechanism (SCDM) and the feed cabin. (b) Star frame, A-B rotator, and Stewart platform in the feed cabin. (c) Schematic diagram of the star frame and the UFM.

At present, FAST is operating safely and efficiently with more than 5300 hours of observations per year, but it fails to observe the center of the Milky Way Galaxy, which is limited by the observation angle (or the so-called tilt angle in astronomy) [7], [8]. Currently, the maximum tilt angle of FAST is only 40°. In order to observe the galactic center, the maximum tilt angle of FAST should be extended to 50°. However, since the heavy rigid structure of the A-B rotator and Stewart platform make the feed cabin weigh up to 30-ton [9], [10], the cable tensions of the SCDM almost reach the safe threshold when the tilt angle is 40°. As a result, for the current FAST, the tilt angle cannot be extended and no additional feed receivers can be added due to the weight limit. Although it is possible to increase the maximum tilt angle in theory by rotating the A-B rotator, the heavy A-B rotator can only achieve a rotation of 18° for ensuring structural strength, and there is no more room for rotation.

Therefore, to meet the new observation requirements of FAST, the following two conditions should be considered: (1) The weight of the feed cabin should be reduced as much as possible, e.g., from 30-ton [10] to 3-ton; (2) The tilt angle must be increased from 40° to 50° for observing the galactic

This work was supported by the National Natural Science Foundation of China under Grant 52205038, 62173316, and 51675501, the Anhui Provincial Natural Science Foundation under Grant 2208085QE149, the Anhui Science Fund for Distinguished Young Scholars under Grant 2108085J32, the China Postdoctoral Science Foundation under Grant 2021M693075, and the State Key Laboratory of Robotics and Systems (HIT) under Grant SKLRS-2021-KF-18. *(Corresponding author: Bin Zhang.)*

[1] Xiaoyan Wang, Bin Zhang, Zhaoyang Li, Xinyu Gao, Fei Zhang, Yifan Ma, and Weiwei Shang are with the Department of Automation, University of Science and Technology of China, Jinzhai Road 96, Hefei 230027, P. R. China (email: wxykd@mail.ustc.edu.cn; bzhanghero@ustc.edu.cn; lzy2001@mail.ustc.edu.cn; gxy198@mail.ustc.edu.cn; zfei@ustc.edu.cn; mayifan@mail.ustc.edu.cn; wwshang@ustc.edu.cn).

[2] Rui Yao, Jia-Ning Yin, Hui Li, Qingge Yang, and Qingwei Li are with CAS Key Laboratory of FAST, National Astronomical Observatories, Chinese Academy of Sciences, Beijing 100101, P. R. China. (email: ryao@nao.cas.cn; jnyin@bao.ac.cn; lihui@bao.ac.cn; qgyang@nao.cas.cn; qwli@nao.cas.cn)

center. Under such a background, our team cooperates with the team of FAST [11] and proposes an upgraded feed mechanism (UFM) to replace the current A-B rotator and Stewart platform, which is actually a reconfigurable cable-driven parallel mechanism (see Fig. 1(c)). Due to the light weight of cables, the UFM is expected to reduce the weight of the feed cabin so as to meet the requirements of tilt angle. Besides, UFM can be reconfigured for different observation tasks to obtain better performance.

For the designed UFM, there are two fundamental but critical problems that need to be handled urgently. One is to analyze the influence of structural parameters on the tilt angle and optimize these parameters to meet the observation requirements within constraints, and the other is to analyze the anti-disturbance ability of the UFM to demonstrate the feasibility of the design. Actually, a weak anti-disturbance ability of the UFM may make cable tensions exceed upper bounds or create control problems [12], [13]. For the first problem, a cable-driven mechanism with large rotational capabilities was proposed and its rotational capability was analyzed in [14], but the structural parameters are not optimized. The effect of different structural parameters on the tilt angle is worth discussing in the optimal design of the UFM, which can provide guidance on the parameter selection. The structural parameters of the FAST have been optimized in [15], [16], but the used catenary cable model of FAST is not suitable for the UFM due to different scales. For the second problem, the disturbance wrenches of the UFM may be seriously caused by winds or the outside SCDM. Generally, experimental methods are used to analyze the influences of disturbance wrenches on the position and orientation of the cable-driven mechanism [17]. However, compared with the traditional experimental verification method based on the actual prototype, a complete numerical simulation algorithm is also necessary, which can be used for the preliminary analysis in the absence of a prototype. Currently, such an algorithm is lacking.

Focus on the above two aspects, we analyze the influence of structural parameters on the tilt angle and realize the dimensional optimization of the UFM with tension constraints. Then, based on the optimized structure, the maximum value of wrenches that the UFM can withstand is calculated, which represents the evaluation of the anti-disturbance ability. Firstly, the structure and working mode of the UFM are introduced. Since the feed cabin moves in the workspace at the low speed of $0 \sim 24$ mm/s, its motion state can be considered as the static equilibrium, so that the static model of the UFM is established. Secondly, by considering the influence of different structural parameters of the UFM on the tilt angle, the parameters that play a major role is chosen to optimize the structural dimension. On this basis, the disturbance increment method is proposed to analyze the anti-disturbance ability. A disturbance wrench that is gradually increasing is applied to the moving platform with the stiffness matrix updated accordingly. Then, combining with the elasticity equation and cable tensions, the maximum value of the disturbance wrench can be obtained. Through

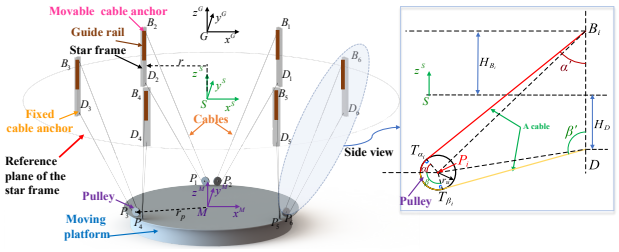

Fig. 2. Schematic diagram of the UFM and geometric relationship between a cable and a pulley.

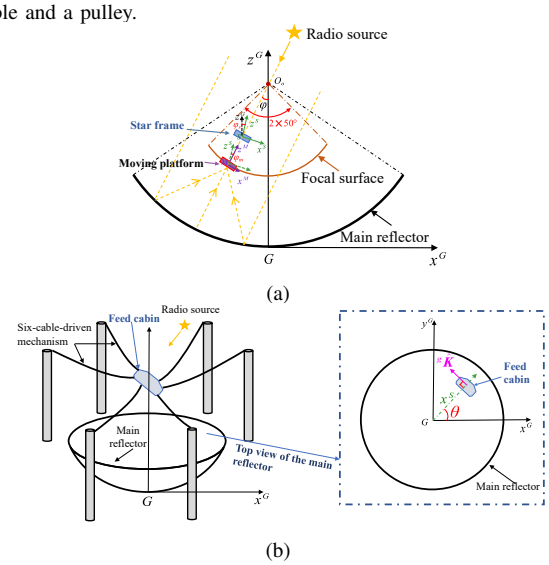

Fig. 3. (a) Schematic diagram of a tilt angle φ. (b) Schematic diagram of an azimuth angle θ, and a unit axis ${}^{g}\hat{\boldsymbol{K}}$.

the above analysis, the results show that it is feasible and reasonable to replace the current A-B rotator and stewart platform in the feed cabin of FAST with the newly-designed UFM, the larger tilt angle can be achieved and the appreciable anti-disturbance ability for long-term stable operation of FAST can be also satisfied.

The rest of this paper is organized as follows. Section II discusses the modeling of the UFM. In Section III, the structural dimension are optimized by considering the tilt angle. The anti-disturbance ability of the UFM is then analyzed in Section IV and the full paper is finally concluded in Section V.

II. Modeling

As shown in Fig. 2, the UFM mainly includes a 6-DOF moving platform, 6 pulleys, 6 cables, 6 fixed cable anchors, 6 movable cable anchors, and 6 guide rails. The movable anchors B_i $(i = 1, ..., 6)$ can slide on the guide rail mounted on the star frame and the cable anchor D_i is fixed on the star frame. Each cable is drawn from the anchor B_i, wrapped around the pulley, and then connected to the anchor D_i. Six cables are used to control the orientation of the moving platform and the configuration of the UFM can be adjusted by changing the positions of the movable cable anchor B_i on the guide rail for obtaining better performance, e.g. for more balanced cable tensions.

A. Working mode of the UFM

In Fig. 2, three coordinate frames are established. A global coordinate frame $G-x^Gy^Gz^G$ is fixed at the bottom center of the reflector, a local coordinate frame $S-x^Sy^Sz^S$ fixed on star frame is established at the plane center of the reference plane, and a local coordinate frame $M-x^My^Mz^M$ fixed on the moving platform is established at the center of gravity of the moving platform.

As shown in Fig. 3(a), when tracking a radio source, both the main reflector and the feed cabin need to be positioned through coordinated motion. Electromagnetic waves are gathered to the focus of the main reflector, and then the feed cabin tracks the focus accurately to achieve high precision reception. Due to the rotation of the Earth, the incident angle of electromagnetic waves will change, and the main reflector also needs to be adjusted for gathering the electromagnetic waves, which will result in many different focuses. All these focuses form a spherical focal surface with the center of curvature O_o. Note that the axis z^M located in the moving platform must point to O_o.

Since the feed cabin consists of the star frame and the UFM, to achieve this pointing motion, it is necessary to rely on the rotation of the star frame and the moving platform of the UFM. T&T (Tilt-and-Torsion) angles [18], namely azimuth, tilt, and torsion angles, are used to describe the orientations in this paper. As shown in Fig. 3(a), under the control of SCDM, the rotation angle of the star frame is the tilt angle φ_s (angle between z^S-axis and z^G-axis), and at the same time, under the control of the cables in the UFM, the rotation angle of the moving platform with respect to the star frame is the tilt angle φ_m (angle between z^M-axis and z^S-axis). Since the UFM is fixed on the star frame, the total tilt angle φ (angle between z^M-axis and z^G-axis) of the moving platform is $\varphi=\varphi_m+\varphi_s$. With the priori experiences and simulations of the FAST team, the relationship between the φ_s and φ is expressed as

$$\varphi_s=\begin{cases} 3\varphi/8, 0^\circ\leqslant\varphi\leqslant 30^\circ \\ -21\varphi^2/1600+93\varphi/80-189/16, 30^\circ\leqslant\varphi\leqslant 90^\circ \end{cases}, \tag{1}$$

In the working mode of UFM, both the star frame and the moving platform have no torsion, and as shown in Fig. 3(b) , the azimuth angle θ ($\theta\in[0,360^\circ]$) is defined as the angle between x^S-axis and x^G-axis, which is positive in anticlockwise direction.

B. Modeling

To represent a rotation matrix, Quaternions are used with a unit axis ${}^g\hat{\boldsymbol{K}}=[k_x\ k_y\ k_z]^T$ and a rotation angle φ_k, hence a unit quaternion is denoted as $\boldsymbol{q}=[q_0\ q_1\ q_2\ q_3]^T$, where $q_0=\cos\frac{\varphi_k}{2}, q_1=k_x\sin\frac{\varphi_k}{2}, q_2=k_y\sin\frac{\varphi_k}{2}, q_3=k_z\sin\frac{\varphi_k}{2}$, and the rotation matrix can be written as

$$\boldsymbol{R}(q_0,q_1,q_2,q_3)= \begin{bmatrix} q_0^2+q_1^2-q_2^2-q_3^2 & 2(q_1q_2-q_0q_3) & 2(q_0q_2+q_1q_3) \\ 2(q_1q_2+q_0q_3) & q_0^2-q_1^2+q_2^2-q_3^2 & 2(q_2q_3-q_0q_1) \\ 2(q_1q_3-q_0q_2) & 2(q_0q_1+q_2q_3) & q_0^2-q_1^2-q_2^2+q_3^2 \end{bmatrix}. \tag{2}$$

When the star frame and the moving platform locate at θ (see Fig. 3(b)), they have the same unit axis: ${}^g\hat{\boldsymbol{K}}=[\cos(\theta-\pi/2)\ \sin(\theta-\pi/2)\ 0]^T=[\sin\theta\ -\cos\theta\ 0]^T$, and have different rotation angles: $\varphi_k=\varphi_s$ and $\varphi_k=\varphi$, respectively. Hence, the rotation matrices of the star frame and moving platform in $G-x^Gy^Gz^G$ are respectively expressed as

$$\begin{aligned} {}^g\boldsymbol{R}_s&=\boldsymbol{R}\left(\cos\tfrac{\varphi_s}{2}\ \sin\theta\sin\tfrac{\varphi_s}{2}\ -\cos\theta\sin\tfrac{\varphi_s}{2}\ 0\right), \\ {}^g\boldsymbol{R}_m&=\boldsymbol{R}\left(\cos\tfrac{\varphi}{2}\ \sin\theta\sin\tfrac{\varphi}{2}\ -\cos\theta\sin\tfrac{\varphi}{2}\ 0\right). \end{aligned} \tag{3}$$

Since the star frame in FAST has a dimension of 7 m, the cables in the UFM are relatively short which can be regarded as straight and of negligible weight. In $S-x^Sy^Sz^S$, the position vectors of cable anchors B_i and D_i are denoted as

$$\begin{aligned} {}^s\boldsymbol{b}_i&=[r\cos(i\pi/3)\ \ r\sin(i\pi/3)\ \ h_{B_i}]^T, \\ {}^s\boldsymbol{d}_i&=[r\cos(i\pi/3)\ \ r\sin(i\pi/3)\ \ h_D]^T, \end{aligned} \tag{4}$$

where h_{B_i} and h_D are the height of B_i and D_i with respect to the origin S of $S-x^Sy^Sz^S$ (see Fig. 2), and r is the distribution radius of B_i and D_i. Since the radius of the pulley is small relative to the dimension of the moving platform, the positions of the two adjacent pulleys can be considered to be the same. Hence, the position vector ${}^m\boldsymbol{p}_i$ in $M-x^My^Mz^M$ of the pulley center P_i is written as

$${}^m\boldsymbol{p}_i=\left[r_p\cos(\lfloor\frac{i-1}{2}\rfloor\frac{2\pi}{3}+\frac{\pi}{2})\ r_p\sin(\lfloor\frac{i-1}{2}\rfloor\frac{2\pi}{3}+\frac{\pi}{2})\ 0\right]^T, \tag{5}$$

where the symbol $\lfloor\rfloor$ represents round down and r_p is the distribution radius of the pulleys on the moving platform. Thus, the position vector ${}^s\boldsymbol{p}_i$ in $S-x^Sy^Sz^S$ is expressed as

$${}^s\boldsymbol{p}_i={}^s\boldsymbol{R}_m{}^m\boldsymbol{p}_i+{}^s\boldsymbol{t}_p={}^g\boldsymbol{R}_s^T{}^g\boldsymbol{R}_m{}^m\boldsymbol{p}_i+{}^s\boldsymbol{t}_p, \tag{6}$$

where ${}^s\boldsymbol{t}_p=[0\ 0\ z_p]^T$ is the distance vector from the origin of $S-x^Sy^Sz^S$ to the origin of $M-x^My^Mz^M$. Since $M-x^My^Mz^M$ is located directly below $S-x^Sy^Sz^S$, z_p is a negative value.

Due to the presence of pulleys, there are two wrap angles α_i and β_i between the cable and the pulley shown in Fig. 2. By geometric relationships, α_i and β_i are expressed as

$$\begin{aligned} \alpha_i=\alpha_i^{'}=&\arcsin\left(r_u/||\overrightarrow{{}^sBP_i}||\right)+ \\ &\arccos\left(\frac{||\overrightarrow{{}^sBD_i}||^2+||\overrightarrow{{}^sBP_i}||^2-||\overrightarrow{{}^sDP_i}||^2}{2||\overrightarrow{{}^sBD_i}||||\overrightarrow{{}^sBP_i}||}\right), \end{aligned} \tag{7}$$

$$\begin{aligned} \beta_i=\beta_i^{'}=&\arcsin(r_u/||\overrightarrow{{}^sDP_i}||)+ \\ &\arccos\left(\frac{||\overrightarrow{{}^sBD_i}||^2+||\overrightarrow{{}^sDP_i}||^2-||\overrightarrow{{}^sBP_i}||^2}{2||\overrightarrow{{}^sBD_i}||||\overrightarrow{{}^sDP_i}||}\right), \end{aligned} \tag{8}$$

where $\overrightarrow{{}^sBP_i}={}^s\boldsymbol{b}_i-{}^s\boldsymbol{p}_i$, $\overrightarrow{{}^sDP_i}={}^s\boldsymbol{d}_i-{}^s\boldsymbol{p}_i$, $\overrightarrow{{}^sBD_i}={}^s\boldsymbol{b}_i-{}^s\boldsymbol{d}_i$, and r_u is the radius of pulleys.

With measuring instruments, ${}^s\boldsymbol{t}_p$, ${}^s\boldsymbol{b}_i$, and ${}^s\boldsymbol{d}_i$ can be obtained. Thus, the cable length L_i is written as

$$L_i=\sqrt{||\overrightarrow{{}^sBP_i}||^2-r_u^2}+\sqrt{||\overrightarrow{{}^sDP_i}||^2-r_u^2}+r_u(\alpha_i+\beta_i). \tag{9}$$

The two tangent points of the cable and pulley are denoted as T_{α_i} and T_{β_i}, reapectively, and the distance vector from

the two tangent points to P_i are expressed as

$$\begin{aligned}\overrightarrow{{}^sPT_{\alpha_i}} &= [r_u\cos(\alpha)\lambda_{xi}, r_u\cos(\alpha)\lambda_{yi}, -r_u\sin(\alpha)]^T,\\ \overrightarrow{{}^sPT_{\beta_i}} &= [r_u\cos(\beta)\lambda_{xi}, r_u\cos(\beta)\lambda_{yi}, r_u\sin(\beta)]^T,\end{aligned} \tag{10}$$

where $\lambda_{xi} = \frac{\overrightarrow{{}^sBP_i}(1)}{\sqrt{\overrightarrow{{}^sBP_i}(1)^2+\overrightarrow{{}^sBP_i}(2)^2}}$, $\lambda_{yi} = \frac{\overrightarrow{{}^sBP_i}(2)}{\sqrt{\overrightarrow{{}^sBP_i}(1)^2+\overrightarrow{{}^sBP_i}(2)^2}}$, with $\overrightarrow{{}^sBP_i}(1)$ and $\overrightarrow{{}^sBP_i}(2)$ as the first and second entries in $\overrightarrow{{}^sBP_i}$, respectively.

Thus, the static equilibrium equation is expressed as

$$\begin{cases}\sum_{i=1}^{6}\boldsymbol{T}_i + m\boldsymbol{g} = \boldsymbol{0}\\ \sum_{i=1}^{6}({}^g\boldsymbol{R}_s{}^s\boldsymbol{R}_m)^m\boldsymbol{p}_i \times \boldsymbol{T}_i = \boldsymbol{0}\end{cases}, \tag{11}$$

where $\boldsymbol{g} = [0\ 0\ -g]^T$ with $g = 9.8$ m/s^2, $\boldsymbol{T}_i = {}^g\boldsymbol{R}_s{}^s\boldsymbol{u}_i T_i$ with ${}^s\boldsymbol{u}_i = \frac{\overrightarrow{{}^sBP_i}+\overrightarrow{{}^sPT_{\alpha_i}}}{||\overrightarrow{{}^sBP_i}+\overrightarrow{{}^sPT_{\alpha_i}}||} + \frac{\overrightarrow{{}^sDP_i}+\overrightarrow{{}^sPT_{\beta_i}}}{||\overrightarrow{{}^sDP_i}+\overrightarrow{{}^sPT_{\beta_i}}||}$. Then, (11) can be further rewritten as

$$\boldsymbol{N}\boldsymbol{T} + \boldsymbol{W} = \boldsymbol{0}, \tag{12}$$

where $\boldsymbol{N} = \begin{bmatrix} {}^g\boldsymbol{R}_s{}^s\boldsymbol{u}_1 & \dots & {}^s\boldsymbol{u}_6 \\ ({}^g\boldsymbol{R}_s{}^s\boldsymbol{R}_m{}^m\boldsymbol{p}_1)\times{}^s\boldsymbol{u}_1 & \dots & ({}^g\boldsymbol{R}_s{}^s\boldsymbol{R}_m{}^m\boldsymbol{p}_6)\times{}^s\boldsymbol{u}_6 \end{bmatrix}$, $\boldsymbol{W} = [m\boldsymbol{g}^T\ \boldsymbol{0}^T]^T$, and $\boldsymbol{T} = [T_1 \dots T_6]^T$. Then the tensions of six cables can be calculated by

$$\boldsymbol{T} = -\boldsymbol{N}^{-1}\boldsymbol{W}. \tag{13}$$

III. Optimization of the Structural Dimensions

A. The calculation of maximum tilt angle

Definition 1: φ_{max} is the maximum tilt angle that the UFM can reach at a specific azimuth angle θ_0 ($\theta_0 \in [0°, 360°]$) in the tension bounds with a set of structural parameters of the UFM.

Firstly, with (13), φ_{max} can be obtained by the following optimization problem, namely

$$\begin{aligned}\varphi_{max} &= \arg\min -\varphi\\ s.t.\ \underline{\boldsymbol{T}} &\leqslant \boldsymbol{T} \leqslant \overline{\boldsymbol{T}},\ \varphi_s < \varphi < 90°, \theta = \theta_0,\end{aligned} \tag{14}$$

where $\underline{\boldsymbol{T}} = \left[\underline{T_1}...\underline{T_6}\right]^T$ and $\overline{\boldsymbol{T}} = \left[\overline{T_1}...\overline{T_6}\right]^T$ are the minimum and maximum tension vectors with $\underline{T_i} = 1000$N and $\overline{T_i} = 10000$N (i=1,..,6) as the minimum and maximum tension of cable i, respectively. Since the moving platform must rotate with respect to the star frame, φ must be greater than φ_s in (1), and considering the overturning of the moving platform, φ must be less than 90°.

In Table I, the structural parameters of the UFM, r_u, z_p, h_{B_i}, h_D, r_p, and r, with their upper and lower bounds are shown. For the UFM, we first selected a set of structural parameters as the preliminary dimensions: $r_u = 0.1$ m, $z_p = -2$ m, $h_{B_i} = 0$, $h_D = -0.72$ m, $r_p = 1.8$ m, $r = 2.8$ m. To simplify and facilitate the solving process, the azimuth θ is discretized with a resolution of 1°, and based on these dimensions, from $\theta_0 = 0°$ to 360°, (14) is repeatedly calculated to get 360 different φ_{max} with the particle swarm optimization algorithm. The results are shown in Fig. 4, where the polar angle and the polar axis represent

TABLE I

Structural Parameters

Parameters	Lower bound (m)	Upper bound (m)
Pulley radius: r_u	$\underline{r_u} = 0.08$	$\overline{r_u} = 0.15$
The third entry in ${}^s\boldsymbol{t}_p$: z_p	$\underline{z_p}$ = -2.3	$\overline{z_p}$ = -1.4
Height of B_i: h_{B_i}	$\underline{h_{B_i}}$ = -0.5	$\overline{h_{B_i}} = 1$
Height of D_i: h_D	$\underline{h_D}$ = -1	$\overline{h_D}$ = -0.7
Distribution radius of pulleys: r_p	$\underline{r_p} = 1.5$	$\overline{r_p} = 2.25$
Distribution radius of $B_i(D_i)$:r	$\underline{r} = 2.5$	$\overline{r} = 3.5$

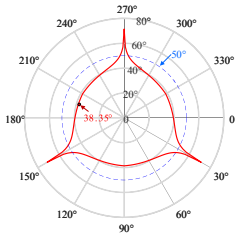

Fig. 4. The values of φ_{max} at different θ_0 ($\theta_0 \in [0°, 1°, 2°, ...360°]$).

the azimuth angle θ and φ_{max}, respectively. It can be seen that the changes of φ_{max} is strongly correlated with θ,

Definition 2: φ_{Max} is the maximum tilt angle that the UFM can reach at all azimuth angles in the tension bounds with a set of structural parameters of the UFM.

To obtain φ_{Max}, the optimization problem is given as

$$\begin{aligned}\varphi_{Max} &= \arg\min_{\theta\in[0°,360°]}\min -\varphi\\ s.t.\ \underline{\boldsymbol{T}} &\leqslant \boldsymbol{T} \leqslant \overline{\boldsymbol{T}},\ \varphi_s < \varphi < 90°.\end{aligned} \tag{15}$$

Thus, φ_{Max} is the minimum one of all the results in (14), and φ_{Max} is only 38.35° shown in Fig. 4, which far less than 50°. In other words, the tilt angle of the UFM with the preliminary dimensions can not reach 50°. Hence, the structural dimension of the UFM should be optimized.

B. Optimization of the structural dimension

Before the optimization, analyzing the influence of these parameters on φ_{Max} can provide reference for dimension optimization. The single variable principle is employed to change the value of only one parameter at a time within its bounds, leaving the other parameters unchanged. Then, the relationship between φ_{Max} and the changes of these parameters are shown in Fig. 5. In Fig. 5(a), although the increase of r_u contributes to the raising of φ_{Max}, it cannot be set too large due to the structural size of the moving platform. From Figs. 5 (b)-(d), with the increase of h_{B_i} and h_D, and the decrease of z_p, φ_{Max} becomes larger. In Figs. 5(e)-(f), when r_p grows, φ_{Max} increases, while r is the opposite case.

Therefore, to improve φ_{Max}, the five influence parameters that play a major role, z_p, h_{B_i}, h_D, r_p, and r, are chosen to optimize structural dimensions by

$$\begin{aligned}&\min_{\theta=0°,1°,...,360°}\left(\min_{z_p,h_{B_i},h_D,r,r_p,} -\varphi\right)\\ &s.t. \underline{\boldsymbol{T}} \leqslant \boldsymbol{T} \leqslant \overline{\boldsymbol{T}},\ \varphi_s < \varphi < 90°\\ &\underline{h_{B_i}} \leqslant h_{B_i} \leqslant \overline{h_{B_i}},\ \underline{h_D} \leqslant h_D \leqslant \overline{h_D},\\ &\underline{r} \leqslant r \leqslant \overline{r},\ \underline{r_p} \leqslant r_p \leqslant \overline{r_p},\ \underline{z_p} \leqslant z_p \leqslant \overline{z_p},\\ &r - r_p \geqslant 0.8\text{ m}, {}^s\boldsymbol{d}_i(3) > {}^s\boldsymbol{p}_i(3).\end{aligned} \tag{16}$$

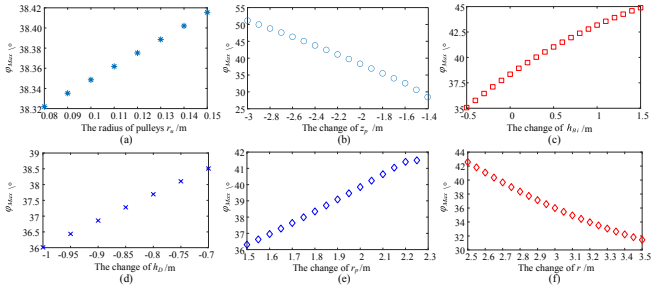

Fig. 5. The influence of parameters on φ_{Max}. (a) Only r_u is changed. (b) Only z_p is changed. (c) Only h_{B_i} is changed. (d) Only h_D is changed. (e) Only r_p is changed. (f) Only r is changed.

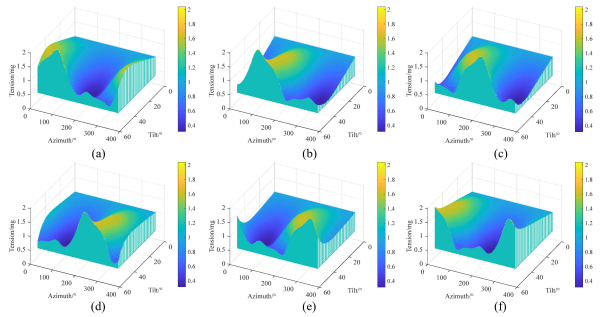

Fig. 6. The tensions of six cables. (a)-(f) represent T_1 to T_6.

To ensure sufficient motion range of the moving platform, $r - r_p \geqslant 0.8$ m, and to maintain a suspended configuration of the UFM, ${}^s\boldsymbol{d}_i(3) > {}^s\boldsymbol{p}_i(3)$. Since (16) is an nonlinear optimization problem with a large number of parameters, the particle swarm optimization algorithm is used to solve it. Then, the result is $\varphi_{Max} = 50.8°$ with $h_{B_i} = 1$m, $h_D = -0.7$m, $r = 2.5$m, $r_p = 1.7$m, $z_p = -2.3$m, which indicates that the UFM can meet observation requirements. With these optimized structural parameters, the tensions of six cables in the whole workspace with discrete values of 1° when $\theta \in [0, 360°]$, $\varphi \in [0, 50°]$ are shown in Figs. 6(a)-(f). Note that the unit of cable tension is the weight "mg" of the moving platform, and the tensions are within bounds in the whole workspace. Besides, the variation of tensions has no sharp changes and spikes.

IV. The Analysis of Anti-Disturbance Ability

During operation, the UFM may suffer from the disturbances from winds or the vibrations of the star frame caused by the outside SCDM. Therefore, an important characteristic of the UFM is that the appreciable anti-disturbance ability for long-term stable operation can be achieved. Hence, in this section, the maximum disturbance wrench that the UFM can withstand is analyzed.

For given θ and φ, suppose that the moving platform is static, then the cable length L_i can be calculated in (9) and the cable tension T_i can be obtained by (13). By considering the elasticity of cable i, the elongation ΔL_i can be got by

$$\Delta L_i = L_i - L_{i0} = L_{i0} T_i / E A_i, \tag{17}$$

where L_{i0} is its original cable length, E is its elastic modulus, and A_i is its cross-sectional area. Then, (17) can be further deduced to get

$$L_{i0} = L_i E A_i / (T_i + E A_i), \tag{18}$$

$$T_i = EA\,(L_i / L_{i0} - 1)\,. \tag{19}$$

Definition 3: The pseudo-drag state, that is, when the static moving platform is located at given θ and φ, the tension $T_i \leqslant 0$ due to the existence of disturbance, at this time the state of the cable is pseudo-drag.

For the convenience of subsequent analysis, $\boldsymbol{X} = [{}^s\boldsymbol{t}_p^T \ \boldsymbol{\phi}^T]^T$ is used to represent the pose of the moving platform with $\boldsymbol{\phi}$ is represented by ZYX Euler angle. By the previous optimization of (16), one gets ${}^s\boldsymbol{t}_p = [0\ 0\ -2.3]^T$m. For given θ and φ, the corresponding $\boldsymbol{\phi}$ can be calculated by the rotation matrices in (3).

The disturbance force and moment acting on the moving platform in $S - x^S y^S z^S$ are denoted as $\boldsymbol{F}_{ext} = [F_{ext}^x \ F_{ext}^y \ F_{ext}^z]^T$, $\boldsymbol{M}_{ext} = [M_{ext}^x \ M_{ext}^y \ M_{ext}^z]^T$, respectively. In order to simulate the disturbance force and moment from all directions, a unit force and moment are respectively defined as $\boldsymbol{f}_{ext} = [\sin\beta_1 \cos\alpha_1 \ \sin\beta_1 \sin\alpha_1 \ \cos\beta_1]^T$, $\boldsymbol{m}_{ext} = [\sin\beta_2 \cos\alpha_2 \ \sin\beta_2 \sin\alpha_2 \ \cos\beta_2]^T$, where $\alpha_1, \alpha_2 \in [0°, 360°]$ and $\beta_1, \beta_2 \in [0°, 180°]$. Hence, the disturbance force and moment can be further written as

$$\boldsymbol{F}_{ext} = ||\boldsymbol{F}_{ext}||\boldsymbol{f}_{ext}, \boldsymbol{M}_{ext} = ||\boldsymbol{M}_{ext}||\boldsymbol{m}_{ext}, \tag{20}$$

where $||\boldsymbol{F}_{ext}||$ and $||\boldsymbol{M}_{ext}||$ are the norm of $\boldsymbol{F}_{ext}$ and $\boldsymbol{M}_{ext}$, respectively. Based on the priori knowledge of FAST, there is a ratio N_r between$||\boldsymbol{F}_{ext}||$ and $||\boldsymbol{M}_{ext}||$:

$$||\boldsymbol{M}_{ext}|| = N_r ||\boldsymbol{F}_{ext}||. \tag{21}$$

The total disturbance wrench is then denoted as $\Delta\boldsymbol{F} = \left[\boldsymbol{F}_{ext}^T \ \boldsymbol{M}_{ext}^T\right]^T$.

A. Disturbance increment method

The disturbance increment method is then adopted to analyze the anti-disturbance ability of the UFM. The disturbance wrench $\Delta\boldsymbol{F}$ is divided into n parts, and then the unit disturbance wrench can be written as: $\delta\boldsymbol{F} = \Delta\boldsymbol{F}/n$. When $\delta\boldsymbol{F}$ is applied to the moving platform, the generated pose offset $\delta\boldsymbol{X}$ can be obtained as

$$\delta\boldsymbol{F} = \boldsymbol{K}(\boldsymbol{X})\delta\boldsymbol{X}, \tag{22}$$

where $\boldsymbol{K}(\boldsymbol{X})$ is the stiffness matrix of the UFM. By appling $\delta\boldsymbol{F}$ to the moving platform repeatedly for n times, the total pose offset $\Delta\boldsymbol{X}$ is $\Delta\boldsymbol{X} = \sum_{j=1}^{n} \delta\boldsymbol{X}$. Hence, the effect of the disturbance wrench $\Delta\boldsymbol{F}$ is simulated. The procedure of the proposed disturbance increment method is given as follows.

Step 1. Given θ and φ, the cable length L_i and the cable tension T_i can be obtained, and then the original cable length L_{i0} is calculated by (18); with (3), one gets the pose $\boldsymbol{X}$; The initial value of $||\boldsymbol{F}_{ext}||$ is set and by picking random values of $\alpha_1, \alpha_2, \beta_1$, and β_2; k different disturbance wrenches are generated to form a wrench set.

Step 2. A wrench $\Delta\boldsymbol{F}$ is extracted from the wrench set.

Step 3. Set $j = 1$ and the small disturbance wrench $\delta\boldsymbol{F} = \Delta\boldsymbol{F}/n$ is acted on the moving platform resulting in a pose offset $\delta\boldsymbol{X} = \boldsymbol{K}^{-1}\delta\boldsymbol{F}$. Update the pose $\boldsymbol{X}_{new}$ with $\boldsymbol{X} + \delta\boldsymbol{X}$

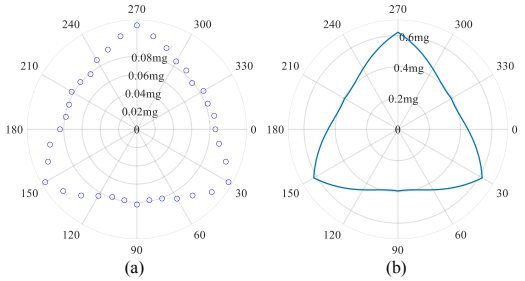

Fig. 7. $\varphi = 30°, \theta \in [0, 360°]$. (a) The norms of the disturbance wrenches. (b) The minimum tensions when the moving platform is not affected by any disturbance wrenches.

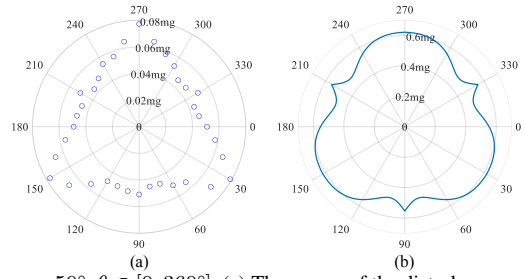

Fig. 8. $\varphi = 50°, \theta \in [0, 360°]$. (a) The norms of the disturbance wrenches. (b) The minimum tensions when the moving platform is not affected by any disturbance wrenches.

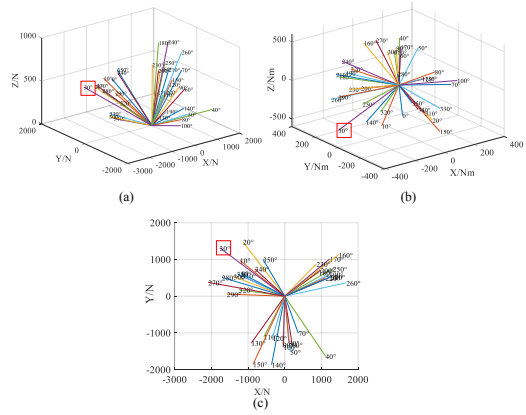

Fig. 9. The maximum disturbance wrenches. (a) The disturbance forces. (b) The disturbance moments. (c) The projection of Fig. 9(a) in xy plane.

and then update the cable length L_i with the new pose $\boldsymbol{X}$. With L_{i0} obtained in **Step 1**, the tension is calculated using (19). If $T_i \leqslant 0$, the maximum disturbance wrench that the moving platform can withstand is $j\delta\boldsymbol{F}$ and then the process can be ended. Otherwise, if $T_i > 0$, $\boldsymbol{K}(\boldsymbol{X}_{new})$ is further calculated and $j \leftarrow j + 1$.

Step 4. Repeat **Step 3** n times. If the maximum disturbance wrench is not found, start over from **Step 2** to **Step 4** until all the k wrenches have been tested.

Step 5. Update the value of $||\boldsymbol{F}_{ext}||$ with $||\boldsymbol{F}_{ext}|| = ||\boldsymbol{F}_{ext}|| + d$ (d is a constant) and start over from **Step 2** until the maximum disturbance wrench is found with $T_i \leqslant 0$.

B. Simulations

In simulations, the above parameters are set as: the elastic modulus $E = 1.6 \times 10^{11}$ Pa, the cross-sectional area $A_i = 5.94 \times 10^{-5}$ m^2, $k = 150$, $N_r = 0.2522$ in (21), $||\boldsymbol{F}_{ext}|| = 0.034$mg, and $d = 0.0017$mg (in **Step 5**).

At $\varphi = 30°$, the maximum disturbance wrench is calculated with a resolution of $10°$ azimuth angle. The norms of the maximum disturbance wrenches at different azimuth angles is shown in Fig. 7(a) with its polar angle represents θ, and its polar axis is a norm of a maximum disturbance wrench expressed by "mg". At $\theta = 30°, 150°, 270°$, the three peaks mean the relatively strong anti-disturbance ability. The minimum norm of these wrenches is 0.079 mg, hence the disturbance wrench that the UFM can withstand is relatively large. When the moving platform is not affected by any disturbance wrenches, tensions T_i at $\theta \in [0, 360°]$, $\varphi = 30°$, are calculated, and then the minimum one among T_i at each azimuth angle θ is counted (see Fig. 7(b)). From the peaks of Fig. 7(a) and 7(b), the variation trend of wrench norms is strongly correlated with that of the minimum tensions.

At $\varphi = 50°$, the norms of the maximum disturbance wrenches at different azimuth angles are shown in Fig. 8(a). Compared Fig. 7(a) with Fig. 8(a), it is found that the anti-disturbance ability of the UFM becomes weaker with the increase of φ. Even at $\varphi = 50°$, the anti-interference ability is sufficient with the minimum norm 0.042 mg of the maximum disturbance. The minimum one among T_i at each azimuth angle θ is counted in Fig. 7(b) when the moving platform is not applied any disturbance wrenches. Similarly, the variation trend of the wrench norms is the same as that of the minimum tensions.

Corresponding to Fig. 8(a), the maximum disturbance wrench (force and moment are expressed separately) at each azimuth angle is counted and represented by a colored segment shown in Fig. 9. The length and direction of a segment represent the magnitude and direction of a maximum disturbance force (moment), respectively. The end of each segment is marked with θ. For example, $\theta = 30°$ marked with a red box indicates that the UFM is located at $\theta = 30°$. In Fig. 9(a), the disturbance forces are mostly in the upward direction while the moments have no obvious directionality in Fig. 9(b). Note that the directions of disturbance forces are related to the structure of the UFM in Fig. 9(c) .

V. Conclusion

In this paper, an upgraded feed mechanism (UFM) is proposed to replace the existing rigid A-B rotator and Stewart platform in the feed cabin of FAST, which can increase the observation angle by reducing weight of the feed cabin. By analyzing the influence of structural parameters on the tilt angle, the main influence parameters are chosen to optimize the dimension of the UFM, which then makes the maximum tilt angle increase from the current $40°$ to the future $50°$. Besides, a novel disturbance increment method is used to analyze the anti-disturbance ability of the UFM. Simulation results indicate that the anti-interference ability becomes weaker with the increase of the tilt angle, but at the maximum tilt angle, the UFM still has the appreciable anti-disturbance ability. Hence, the UFM can not only realize the weight reduction, so as to expand the observation range of FAST, but also achieve long-term stable operation performance. In the future, we will build a real prototype of the UFM to experimentally verify the effectiveness of the upgrade in FAST.

REFERENCES

[1] T. C. Ching, D. Li, C. Heiles, Z. Y. Li, L. Qian, Y. L. Yue, J. Tang, and S. H. Jiao, "An early transition to magnetic supercriticality in star formation," *Nature*, vol. 601, pp. 49-52, Jan. 2022.

[2] L. Lin, C. F. Zhang, P. Wang, H. Gao, X. Guan, *et al.*, "No pulsed radio emission during a bursting phase of a Galactic magnetar," *Nature*, vol. 587, pp. 63-65, Nov. 2020.

[3] D. Li, P. Wang, W. W. Zhu, B. Zhang, X. X. Zhang, *et al.*, "A bimodal burst energy distribution of a repeating fast radio burst source," *Nature*, vol. 598, pp. 267-271, Oct. 2021.

[4] R. Luo, B. J. Wang, Y. P. Men, C. F. Zhang, J. C. Jiang, *et al.*, "Diverse polarization angle swings from a repeating fast radio burst source," *Nature*, vol. 586, pp. 693-696, Oct. 2020.

[5] D. Li and Z. C. Pan, "The five-hundred-meter aperture spherical radio telescope project," *Radio Sci.*, vol. 51, no.7, pp. 1060-1064, Jul. 2016.

[6] P. Jiang, Y. L. Yue , H. Q. Gan, R. Yao, H. Li, *et al.*, "Commissioning progress of the FAST," *Sci. China-Phys. Mech. Astron.*, vol. 62, no. 5, pp. 1-22, May 2019.

[7] E. Abdalla, E. G. M. Ferreira, R. G. Landim, A. A. Costa, K. S. F. Fornazier, *et al.*, "The BINGO project: I. Baryon acoustic oscillations from integrated neutral gas observations," *Astron. Astrophys.*,vol. 664, Aug. 2022, Art. no. A14.

[8] H. M. Tedila, R. Yuen, N. Wang, J. P. Yuan, Z. G. Wen, *et al.*, "Emission variation of a long-period pulsar discovered by the five-hundred-meter aperture spherical radio telescope (FAST)," *Astrophys. J.*, vol. 929, no. 2, Apr. 2022, Art. no. 171.

[9] J. N. Yin, P. Jiang, and R. Yao, "An approximately analytical solution method for the cable-driven parallel robot in FAST," *Res. Astron. Astrophys.*, vol. 21, no. 2, Mar. 2022.

[10] R. Yao, C. H. Fu, C. H. Sun, and W. B. Zhu, "Accuracy design of the stewart manipulator of the five-hundred-meter aperture spherical radio telescope," *Adv. Mech. Eng.*, vol. 11, no. 4, Apr. 2019.

[11] H. Li and R. Yao, "Optimal orientation planning and control deviation estimation on FAST cable-driven parallel robot," *Adv. Mech. Eng.*, vol. 6, pp. 1-7, May 2014.

[12] H. Jamshidifar, S. Khosravani, B. Fidan, and A. Khajepour, "Vibration decoupled modeling and robust control of redundant cable-driven parallel robots," *IEEE/ASME Trans. Mechatronics*, vol. 23, no. 2, pp. 690-701, Apr. 2018.

[13] R. Babaghasabha, M. A. Khosravi, and H. D. Taghirad, "Adaptive robust control of fully-constrained cable driven parallel robots," Mechatronics, vol. 25, pp. 27-36, Feb. 2015.

[14] E. Idà, D. Marian, and M. Carricato, "A deployable cable-driven parallel robot with large rotational capabilities for laser-scanning applications," *IEEE Robot. Autom. Lett.* , vol. 5, no. 3, pp. 4140-4147, Jul. 2020.

[15] B. Y. Duan, Y. Y. Qiu, F. S. Zhang, and B. Zi, "On design and experiment of the feed cable-suspended structure for super antenna," *Mechatronics*, vol. 19, no. 4, pp. 503-509, Jun. 2009.

[16] R. Yao, X. Q. Tang, J. S. Wang, and P. Huang, "Dimensional optimization design of the four-cable-driven parallel manipulator in FAST," *IEEE/ASME Trans. Mechatronics*, vol. 15, no. 6, pp. 932-941, Dec. 2010.

[17] S. H. Hou, X. Q. Tang, H. N. Sun, Y. H. Wang, and Q. Z. Li, "Analysis of cable-force transmission characteristics and disturbing force/moment of high-acceleration cable-driven parallel mechanism," *IEEE/ASME Trans. Mechatronics*, vol. 27, no. 1, pp. 348-359, Feb. 2022.

[18] I. A. Bonev, "Geometric analysis of parallel mechanisms," Ph.D. thesis, Laval University, Canada, 2002.